LHCb Note 2008-012
PHYSICS

Impact of misalignments on the analysis of B decays

M. Gersabeck, E. Rodrigues

University of Glasgow, U.K.

J. Nardulli

Rutherford Appleton Laboratory, Didcot, U.K.

August 2008

Abstract

This note investigates the effects of a misaligned tracking system on the analysis of B decays. Misalignment effects of both the vertex locator and the inner and outer T-stations have been studied. z-scaling effects of the vertex locator are also considered. It is shown that misalignments of the order of one third of the detector single-hit resolutions have little or negligible effects on the quality of the reconstruction and of the analysis of B decays. The studies were performed with a sample of $B^0_{(s)} \to h^+h'^-$ decays, but the impact of misalignments on the performance of the pattern recognition algorithms and on the primary vertex resolutions, assessed for the first time, are rather general and not restricted to $B^0_{(s)} \to h^+h'^-$ decays.

Contents

1 Introduction and motivation

An accurate and efficient tracking system is of crucial importance to the success of the LHCb experiment [1, 2]. The alignment of the tracking system is of great importance, as misalignments potentially cause losses in both tracking and physics performances.

Understanding the alignment of the tracking detector planes is of paramount importance in track reconstruction. This can be schematically demonstrated with the simple example shown in Figure 1. Here, a particle passes through a misaligned detector (left panel), but is fitted assuming the uncorrected geometry (right panel). As a consequence, wrong hit positions are assigned to the track and the tracking performance deteriorates.

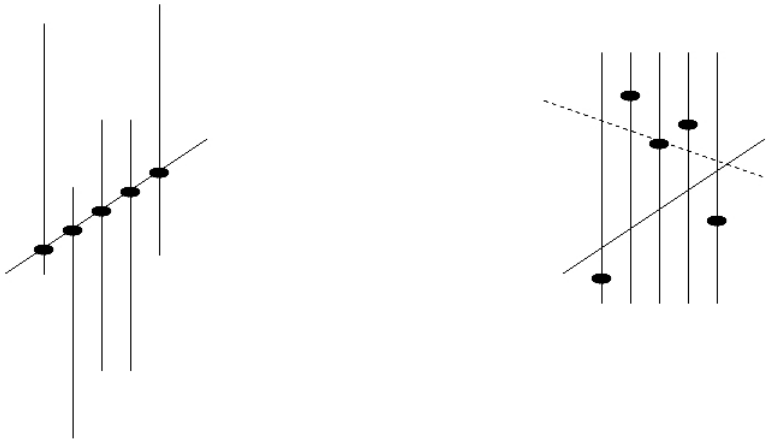

Figure 1: The basic alignment problem: a particle passes through a misaligned detector (left) but is fitted using the uncorrected geometry (right). Both the "true" track (full line) and the "mis-reconstructed" track (dashed line) are visible.

First studies of the deterioration of the LHCb tracking and (software) trigger performance due to residual misalignments in the Vertex Locator (VELO) were discussed in [3] [1]. A study of the consequences of a misaligned Outer Tracker on the signal and background separation of $B^0_{(s)} \to h^+h'^-$ decays can be found in [4].

Here, the effects of misalignments of both the Vertex Locator and the tracking T-stations on the analysis of the $B^0_{(s)} \to h^+h'^-$ decays are investigated in detail. Not only the effects on the pattern recognition, but also on the event selection and reconstruction performance are described.

It is important to emphasise that the systematic study presented in this note aims at assessing the effect of misalignments purely based on their size.

[1] Note that these studies relate to a rather old and obsolete version of the trigger.

Detector	Translations (μm)			Rotations (mrad)		
	Δ_x	Δ_y	Δ_z	R_x	R_y	R_z
VELO modules	3	3	10	1.00	1.00	0.20
VELO sensors	3	3	10	1.00	1.00	0.20
IT boxes	15	15	50	0.10	0.10	0.10
OT layers	50	0	100	0.05	0.05	0.05

Table 1: Misalignment "1σ" scales for the VELO modules and sensors, the IT boxes and OT layers.

The next section details the implementation of misalignments and the data samples used for the study. Section 3 presents the impact of misalignments on the analysis of $B^0_{(s)} \to h^+h'^-$ decays separately for several "classes" of misalignments of the tracking detectors VELO, Inner Tracker (IT) and Outer Tracker (OT). The conclusion and areas of future work are discussed in Section 4.

2 Implementation of misalignments

2.1 Misalignment scales

As mentioned in the previous section, here the effects of misalignments based solely on their magnitude are considered. In particular, no assumptions are made based on the quality of the metrology or the expected performance of the alignment algorithms.

The misalignment effects are looked at as a function of a "misalignment scale". The scales were chosen to be roughly $1/3$ of the detector single-hit resolution – called "1σ". Misalignments were then applied to each VELO module and sensor, each IT box and OT layer following a Gaussian distribution with a sigma corresponding to the 1σ values. The list of these misalignment 1σ scales is summarised in Table 1. Figure 2 graphically confirms the Gaussian distributions with some examples.

For each sub-detector 10 sets of such 1σ misalignments were generated, to avoid any potentially "friendly" or "catastrophic" set of misalignments. Likewise, this procedure was repeated with the creation of 10 similar sets for each VELO module and sensor and each IT box and OT layer with misalignment scales increased by factors of 3 (3σ) and 5 (5σ).

Each of these 10 misalignment sets were implemented and stored in dedicated (conditions) databases. In total 9 databases were produced, corresponding to the 1σ, 3σ and 5σ misalignments for the VELO, IT and OT detectors.

2.2 Data samples

The study was performed with a $20k$ sample of $B^0 \to \pi^+\pi^-$ events [2] for each scenario:

- perfect alignment (denoted 0σ in the rest of the note);
- 1σ, 3σ and 5σ misalignments for the following cases:
  VELO misalignments, IT and OT misalignments, and misalignments of VELO, IT and OT.

Each $20k$ sample consists in reality of 10 sub-samples of $2k$ events, each of which was processed with a different one of the 10 sets of a particular misalignment scenario. In addition, the effects of a systematic change in the VELO z-scale have also been studied.

2.3 Event processing

All the events were generated and digitized with a perfect geometry (`Gauss` generation program version v25r8 and `Boole` digitization program version v12r10). Starting always from the same digitized data samples, the misalignments were only introduced at reconstruction level, where pattern recognition, track fitting, primary vertexing and particle identification are performed. The version `v32r2` of the `Brunel` reconstruction software was used for this task. Physics analysis was later performed with the `DaVinci` program version `v19r9`.

3 Impact of misalignments on the analysis of $B^0_{(s)} \to h^+h'^-$ decays

In this section the direct effect of misalignments on the selection of the $B^0_{(s)} \to h^+h'^-$ decays (as extensively described in [5]) is analysed. First, the misalignments of the VELO are considered (in Section 3.1), then the ones of the IT and OT tracking stations (in Section 3.2). Next the combined effects of both the VELO and the tracking stations were considered (in Section 3.3). The last subsection, 3.4, is devoted to the analysis of effects of z-scaling of the VELO detector.

In all four studies, first the effect of misalignments on the pattern recognition algorithms efficiencies is described, subsequently the effect on the event selection is considered and every single cut is described in detail. Finally, the variations of momentum and B^0 mass, vertex and proper time resolutions are shown as a function of the misalignments.

[2] For the sake of simplicity only one of the $B^0_{(s)} \to h^+h'^-$ family of decays was considered, as their different final states and B-mother are not relevant in the present study.

In Table 2 the selection cuts applied to the $B^0_{(s)} \to h^+h'^-$ channels are shown. A more detailed explanation of all cuts can be found in [5].

$B^0_{(s)} \to h^+h'^-$ selection parameter	cut value
smallest p_t(GeV) of the daughters	> 1.0
largest p_t(GeV) of the daughters	> 3.0
$B^0_{(s)}$ p_t(GeV)	> 1.2
smallest IP/σ_{IP} of the daughters	> 6
largest IP/σ_{IP} of the daughters	> 12
$B^0_{(s)}$ IP/σ_{IP}	< 2.5
$B^0_{(s)}$ vertex fit χ^2	< 5
$(L)/\sigma_L$	> 18
$\|\Delta$m$\|$(MeV)	< 50

Table 2: Selection cuts applied to the $B^0_{(s)} \to h^+h'^-$ channels.

3.1 Misalignments in the VELO

3.1.1 Effect on the pattern recognition

Once the misalignments are introduced at the reconstruction level, as explained in Section 2, their effects need to be studied both on the pattern recognition (track finding efficiencies) and on the event selection (efficiency for finding the correct decay).

The pattern recognition algorithms [3] considered are the ones that find:

- tracks in the VELO detector in r-z and 3D-space. The algorithms are hereafter denoted by `VeloR` and `VeloSpace`, respectively;
- tracks that traverse the whole LHCb detector (called "long tracks"). The two existing long tracking algorithms are hereafter denoted `Forward` and `Matching`.

In Table 3 the efficiencies for the `VeloR`, `VeloSpace`, `Forward`, and `Matching` pattern recognition algorithms are shown for the 0σ, 1σ, 3σ and 5σ scenarios. All efficiencies are quoted for all long tracks in the event with no momentum cut applied.

A clear relative degradation of 6.1% for the `VeloSpace` track finding efficiency is observed in the 5σ scenario. For the 1σ scenario there is hardly any effect. The deterioration

[3] For more details about the definitions of the pattern recognition efficiencies see [6].

in the Forward and Matching long tracking efficiencies can be fully attributed to the worsening in the VELO part. Hence, these algorithms are not directly affected by VELO misalignments, as expected.

All pattern recognition efficiencies quoted throughout the note refer to averages obtained from the 10 sub-samples explained in Section 2. Further details are discussed in Appendix A.

Misalignment scenario	VeloR efficiency (%)	VeloSpace efficiency (%)	Forward efficiency (%)	Matching efficiency (%)
0σ	98.0 ± 0.1	97.0 ± 0.1	85.9 ± 0.2	81.1 ± 0.2
1σ	98.0 ± 0.1	96.7 ± 0.1	85.6 ± 0.2	80.9 ± 0.2
3σ	98.0 ± 0.1	93.9 ± 0.8	83.1 ± 0.6	78.3 ± 0.6
5σ	97.7 ± 0.2	91.1 ± 1.7	80.1 ± 1.6	75.5 ± 1.5

Table 3: VeloR, VeloSpace, Forward and Matching pattern recognition efficiencies for a perfectly aligned VELO and various VELO misalignment scenarios.

3.1.2 Effect on the event selection

In this section the effect of misalignments of the VELO on the various discriminating variables shown in Table 2 is analysed.

In this instance it is important to realise that the selection cuts on these discriminating variables were optimized for a perfect alignment. It may be that the deteriorations reported hereafter can be reduced to some extent with a cuts re-optimization for the non-perfectly aligned scenarios. This same comment holds for all the studies summarised in the remainder of the note.

In Figures 3 and 4 the distributions of the discriminating variables are shown for the 0σ, 1σ, 3σ and 5σ cases. In each plot the full line represents the 0σ case; the dashed line represents the 1σ case; the dotted line represents the 3σ case and the dot-dashed line represents the 5σ case. Note that all plots are obtained after applying the full selection on all the variables but the plotted one. The cut value is indicated by a vertical line. In case of the p_T and impact parameter significance cuts on the pions, where one threshold is applied to both pions and another has to be exceeded by at least one of them, the common threshold is depicted by a solid line, while the additional threshold is shown as a dashed line. In addition, normalised integrals are shown to give a direct comparison of the acceptances for different misalignments [4].

[4]In case of the p_T and impact parameter significance cuts, which have been switched off simultane-

The most sensitive variable to VELO misalignments is the impact parameter significance of the B^0 (Figure 3(a)). The acceptance of this cut drops by a factor two for misalignments as large as in the 5σ case. Other discriminating variables that are affected by VELO misalignments are the B^0 decay vertex χ^2 (relative loss $\approx 30\%$) and the daughters' impact parameter significance (relative loss $< 10\%$). The overview of the number of selected events is given in Table 4.

Misalignment scenario	Number of selected events
0σ	4141 (100%)
1σ	3829 (92.5%)
3σ	2194 (53.0%)
5σ	1082 (26.1%)

Table 4: Number of selected events after running the $B^0_{(s)} \to h^+h'^-$ selection for the different VELO misalignment scenarios.

3.1.3 Effect on resolutions

After having studied the effect of misalignments on the event selection it is equally important to evaluate their impact on physics analysis observables; therefore, momentum and mass resolution have been studied as well as the resolutions on the primary and secondary (B^0 decay) vertices and on the proper time. These resolutions are shown in Figures 5 and 6 while their values (the sigmas of single-Gaussian fits) are summarised in Tables 5 and 6.

The momentum and mass resolutions are only affected on the percent level by VELO misalignments, while the vertex related quantities are strongly affected. For the latter the resolutions worsen by roughly a factor two for the 5σ case compared to the fully aligned scenario. Note that, in particular, the results on the precision of the reconstruction of primary vertices are fully general and not restricted to $B^0_{(s)} \to h^+h'^-$ decays.

In addition to the "bare" resolutions, the effect of misalignments on the assigned proper time error has been studied. Figure 7 shows the distribution of the proper time error for the various misalignment scenarios as well as the respective pull distributions. It is clearly visible and confirmed by the numbers in Table 7 that even in the aligned case there is a bias in the estimation of the proper time and that the errors are under-estimated. With misalignments both the bias and the error estimation worsen significantly. Note that the

ously, the acceptance related to the second cut can not be directly read off the acceptance functions.

Misalignment scenario	Momentum resolution (%)	Mass resolution (MeV)	Proper time resolution (fs)
0σ	0.49	22.5	37.7
1σ	0.50	22.5	39.4
3σ	0.52	22.2	58.1
5σ	0.52	23.5	82.0

Table 5: Values of the resolutions on the daughters' momentum, the B^0 mass and the B^0 proper time for the different VELO misalignment scenarios. The resolutions correspond to the sigmas of single-Gaussian fits. The errors on all resolutions are around 1-1.5 %.

Misalignment scenario	Primary vertex resolutions (μm)			B^0 vertex resolutions (μm)		
	x	y	z	x	y	z
0σ	9	9	41	14	14	147
1σ	10	10	48	15	15	155
3σ	16	16	81	21	21	226
5σ	23	27	147	28	29	262

Table 6: Values of the position resolutions on the primary and the B^0 decay vertices for the different VELO misalignment scenarios. The resolutions correspond to the sigmas of single-Gaussian fits. The errors on all resolutions are around 1-2 %.

errors used in the pull distributions do not account for the change in the effective single-hit resolution due to misalignments. Hence, these figures should only be seen as another way of illustrating the degrading precision as a function of misalignments.

Misalignment scenario	Mean	Sigma
0σ	0.06 ± 0.02	1.14 ± 0.01
1σ	0.09 ± 0.02	1.20 ± 0.01
3σ	0.09 ± 0.03	1.62 ± 0.02
5σ	0.18 ± 0.04	2.08 ± 0.03

Table 7: Values for the mean and sigma of the proper time pulls for the different VELO misalignment scenarios.

3.2 Misalignments in the T stations

3.2.1 Effect on the pattern recognition

In Table 8 both the `Matching` and the `Forward` pattern recognition efficiencies are shown for the 0σ, 1σ, 3σ and 5σ scenarios. Again, all efficiencies are quoted for all long tracks in the event with no momentum cut applied. It can be seen that for the set of misalignments considered there is a relative loss, for the 5σ case, of 0.6% for the `Forward` efficiency and of 5% for the `Matching` efficiency.

Misalignment scenario	`Forward` efficiency (%)	`Matching` efficiency (%)
0σ	85.9 ± 0.2	81.1 ± 0.2
1σ	85.8 ± 0.2	81.0 ± 0.2
3σ	85.6 ± 0.2	79.9 ± 0.4
5σ	85.4 ± 0.3	77.2 ± 1.3

Table 8: `Matching` and `Forward` pattern recognition efficiencies for various misalignment scenarios of the T-stations.

3.2.2 Effect on the event selection

In this section the effect of misalignments of the T-stations on the various discriminating variables shown in Table 2 is analysed.

In Figures 8 and 9 the distributions of the discriminating variables are shown for the 0σ, 1σ, 3σ and 5σ cases (refer to Section 3.1.2 for an explanation of the distributions, lines and cuts applied).

None of the discriminating variables is strongly affected by the misalignments considered. This explains the relatively small – compared to the VELO case – loss in number of selected events, shown in Table 9, which amounts to 4.2% in the worst-case scenario.

3.2.3 Effect on resolutions

In Figures 10 and 11 the B^0 daughters' momentum, B^0 mass and proper time and primary vertex and B^0 vertex resolutions are shown for the 0σ, 1σ, 3σ and 5σ cases. The values of the resolutions (the sigmas of single-Gaussian fits) are summarised in Tables 10 and 11.

Misalignment scenario	Number of selected events
0σ	4141 (100%)
1σ	4131 (99.8%)
3σ	4095 (98.9%)
5σ	3969 (95.8%)

Table 9: Number of selected events after running the $B^0_{(s)} \to h^+h'^-$ selection for the different T-stations misalignment scenarios.

Misalignment scenario	Momentum resolution (%)	Mass resolution (MeV)	Proper time resolution (fs)
0σ	0.49	22.5	37.7
1σ	0.50	22.6	37.4
3σ	0.54	23.4	37.4
5σ	0.59	25.8	38.8

Table 10: Values of the resolutions on the daughters' momentum, the B^0 mass and the B^0 proper time for the different T-stations misalignment scenarios. The resolutions correspond to the sigmas of single-Gaussian fits. The errors on all resolutions are around 1-1.5 %.

Hardly any effect is visible on either the primary and B^0 decay vertex resolutions or on the B^0 proper time resolution. This is expected because the resolution on these quantities

Misalignment scenario	Primary vertex resolutions (μm)			B^0 vertex resolutions (μm)		
	x	y	z	x	y	z
0σ	9	9	41	14	14	147
1σ	9	9	42	14	14	146
3σ	9	9	42	14	14	145
5σ	9	9	42	14	14	142

Table 11: Values of the position resolutions on the primary and the B^0 decay vertices for the different T-stations misalignment scenarios. The errors on all resolutions are around 1-2 %.

is dominated by the VELO resolutions and alignment. On the contrary, a 17% effect can be seen on the momentum resolution of the daughters and a 15% effect on the B^0 invariant mass. Being a two-body decay, the B^0 invariant mass resolution is dominated by the momentum resolution of the daughters, which explains the effect on the B^0 mass resolution.

The effect of misalignments on the proper time error has also been studied. Figure 12 shows the distribution of the proper time error for the various misalignment scenarios as well as the respective pull distributions. As already shown in the VELO case, Section 3.1.3, it can be observed that even in the aligned case there is a bias in the estimation of the proper time and that the errors are under-estimated (see Table 12). No significant worsening is observed in case of misalignments.

Misalignment scenario	Mean	Sigma
0σ	0.06 ± 0.02	1.14 ± 0.01
1σ	0.06 ± 0.02	1.14 ± 0.01
3σ	0.06 ± 0.02	1.15 ± 0.01
5σ	0.05 ± 0.02	1.17 ± 0.01

Table 12: Values for the mean and sigma of the proper time pulls for the different T-stations misalignment scenarios.

3.3 Misalignments in the VELO and T stations

3.3.1 Effect on the pattern recognition

In Table 13 the VeloR, VeloSpace, Forward and Matching pattern recognition efficiencies for all long tracks in the event with no momentum cut applied are shown for the 0σ, 1σ, 3σ and the 5σ scenarios. For the set of misalignments considered there is a relative loss of 8.6% for the Forward efficiency and of 12.9% for the Matching efficiency. These numbers roughly correspond to the combined losses due to the misalignments applied independently in the VELO and in the T-stations, shown in the previous subsections. This indicates that the two effects are largely uncorrelated.

Misalignment scenario	VeloR efficiency (%)	VeloSpace efficiency (%)	Forward efficiency (%)	Matching efficiency (%)
0σ	98.0 ± 0.1	97.0 ± 0.1	85.9 ± 0.2	81.1 ± 0.2
1σ	98.0 ± 0.1	96.8 ± 0.1	85.6 ± 0.2	80.8 ± 0.2
3σ	98.0 ± 0.1	94.3 ± 0.4	83.3 ± 0.5	77.3 ± 0.7
5σ	97.8 ± 0.2	90.1 ± 1.7	78.5 ± 1.8	70.6 ± 1.9

Table 13: VeloR, VeloSpace, Forward and Matching pattern recognition efficiencies for various misalignment scenarios of both the VELO and the T-stations.

3.3.2 Effect on the event selection

In Table 14 the number of selected events is shown for the different misalignment scenarios of both the VELO and the T-stations.

As already shown, if only the T-stations misalignments are considered, the loss in the number of selected events amounts to 4.2%, while in the VELO case, the loss in number of selected events amounts to 73.9%. It can be concluded that the 75.6% loss in number of selected events, here seen in the worst-case scenario, is mostly due to losses induced by misalignments in the VELO. Therefore the distributions of the single-cut variables of the selection have not been studied again.

It should be kept in mind that though the effects of misalignments on the performance of the particle identification have not been studied here, the latter is expected to be influenced mainly by T-stations misalignments.

Misalignment scenario	Number of selected events
0σ	4141 (100%)
1σ	3807 (91.9%)
3σ	2041 (49.3%)
5σ	1009 (24.4%)

Table 14: Number of selected events after running the $B^0_{(s)} \to h^+h'^-$ selection for the different misalignment scenarios of both the VELO and the T-stations considered.

3.3.3 Effect on resolutions

In Figures 13 and 14 the B^0 daughters' momentum, B^0 mass and proper time and primary vertex and B^0 vertex resolutions are shown for the 0σ, 1σ, 3σ and 5σ cases. The values of the resolutions (the sigmas of single-Gaussian fits) are summarised in Tables 15 and 16.

Misalignment scenario	Momentum resolution (%)	Mass resolution (MeV)	Proper time resolution (fs)
0σ	0.49	22.5	37.7
1σ	0.50	22.3	40.9
3σ	0.56	25.1	58.0
5σ	0.63	25.5	78.6

Table 15: Values of the resolutions on the daughters' momentum, the B^0 mass and the B^0 proper time for the different misalignment scenarios of both the VELO and the T-stations. The resolutions correspond to the sigmas of single-Gaussian fits. The errors on all resolutions are around 1-1.5 %.

Comparing these results with the ones previously shown for independent misalignments of the VELO and of the T-stations, it can be seen that while VELO misalignments strongly influence the primary and the B^0 vertex resolutions, and consequently the proper time resolution, T-stations misalignments have an effect on the daughters' momentum resolution and therefore on the B^0 mass resolution. Both misalignments have complementary effects.

Misalignment scenario	Primary vertex (resolutions μm)			B^0 vertex resolutions (μm)		
	x	y	z	x	y	z
0σ	9	9	41	14	14	147
1σ	10	10	48	15	15	159
3σ	14	17	84	20	21	214
5σ	23	27	153	26	31	260

Table 16: Values of the position resolutions on the primary and the B^0 decay vertices for the different misalignment scenarios of both the VELO and the T-stations. The errors on all resolutions are around 1-2 %.

Finally, the effect of misalignments on the proper time error has been studied (see Table 17). Figure 15 shows the distribution of the proper time error for the various misalignment scenarios as well as the respective pull distributions. Again, a bias is observed in the estimation of the proper time, and the proper time errors are under-estimated. Comparing these results with the ones previously shown in Tables 7 and Table 12, it can be concluded that these results strongly resemble the ones in Table 7, indicating that the worsening seen here is originated by the misalignments in the VELO.

Misalignment scenario	Mean	Sigma
0σ	0.06 ± 0.02	1.14 ± 0.01
1σ	0.05 ± 0.02	1.22 ± 0.02
3σ	0.11 ± 0.04	1.63 ± 0.03
5σ	0.15 ± 0.07	2.10 ± 0.06

Table 17: Values for the mean and sigma of the proper time pulls for the different misalignment scenarios of both the VELO and the T-stations.

3.4 Effects of changes in the VELO z-scale

In addition to studying the effects of random misalignments, the change of the VELO z-scale has been examined. This is of particular interest to lifetime measurements as it potentially directly introduces a bias in the measured proper time.

A z-scaling effect could be expected from an expansion due to temperature variations of the VELO components, particularly the Aluminium base plate onto which the individual modules are screwed. However, the base plate is kept constant at $20^{\circ}\mathrm{C}$ by additional local heating. In addition, the scaling should be limited by the carbon-fibre constraint system that keeps the modules in place with a precision of $100\ \mu\mathrm{m}$ and which is less prone to temperature-induced expansion given its material[5].

To assess the influence of an incorrect knowledge of the VELO z-scale, four scenarios with different z-scales have been simulated and studied. For each scenario the z-position of each module has been changed according to the equation

$$z_{module} \rightarrow z_{module} \cdot (1 + scale), \tag{1}$$

where $scale$ takes the four values $\frac{1}{3}10^{-4}$, 10^{-4}, $\frac{1}{3}10^{-3}$, and 10^{-3} for the four scenarios, respectively.

3.4.1 Effect on the pattern recognition

The first quantities to be studied with a changed VELO z-scale were the pattern recognition efficiencies. As shown in Table 18 no deterioration has been observed up to a change in the z-scale of $1/3 \times 10^{-3}$. This is expected for the VELO-based pattern recognitions as a z-scaling effectively only changes the track slopes. For the largest z-scaling under study small losses in the VELO-based pattern recognition efficiencies are observed. These also propagate to the `Forward` and `Matching` efficiencies.

3.4.2 Effect on the event selection

When studying the influence of various z-scales on the event selection the situation observed for the pattern recognition performances repeats itself. The overview of the number of selected events is given in Table 19. The first four scales under study show only a minor loss in the number of selected events, while a relative loss of about 20% is observed for the largest z-scale. As for the studies in the previous chapters, this is due to a worsening in the resolution of the various cut parameters, where particularly the VELO-related quantities have shown great sensitivity.

[5] A conservative estimate using a temperature change of 10 K yields a scaling in the z-direction of 2×10^{-5}. The 10 K are estimated as a maximal change in the temperature of the constraint system as it has a large area contact to the base plate at $20^{\circ}\mathrm{C}$ and only a small cross-section with the VELO modules at about $-5^{\circ}\mathrm{C}$.

z-scale	`VeloR` efficiency (%)	`VeloSpace` efficiency (%)	`Forward` efficiency (%)	`Matching` efficiency (%)
1.00000	98.0	97.0	85.9	81.1
1.00003	98.0	97.0	85.9	81.2
1.00010	98.0	97.0	85.9	81.2
1.00033	98.0	96.8	85.7	81.0
1.00100	96.5	94.3	83.8	79.0

Table 18: `VeloR`, `VeloSpace`, `Forward` and `Matching` pattern recognition efficiencies for the various VELO z-scaling misalignment scenarios.

z-scale	Number of selected events
1.00000	4141 (100.0%)
1.00003	4137 (99.9%)
1.00010	4142 (100.0%)
1.00033	4063 (98.1%)
1.00100	3273 (79.0%)

Table 19: Number of selected events after running the $B^0_{(s)} \to h^+ h^{'-}$ selection for the various VELO z-scaling misalignment scenarios.

3.4.3 Effect on resolutions

The effect of an incorrectly known VELO z-scale on the resolutions of various physics quantities is summarised in Tables 20 and 21. The relevant resolution distributions are pictured in Figures 16 and 17.

For the first three z-scaling scenarios the observed changes in the resolutions are minimal. Only for the two largest z-scaling cases one observes a sizeable deterioration in particular of the proper time and vertex resolutions.

z-scale	Momentum resolution (%)	Mass resolution (MeV)	Proper time resolution (fs)
1.00000	0.49	22.5	37.7
1.00003	0.49	22.2	37.7
1.00010	0.49	22.1	37.7
1.00033	0.49	22.0	38.5
1.00100	0.50	22.0	46.8

Table 20: Values of the resolutions on the daughters' momentum, the B^0 mass and the B^0 proper time for the various VELO z-scaling misalignment scenarios. The resolutions correspond to the sigmas of single-Gaussian fits. The errors on all resolutions are around 1-1.5 %.

z-scale	Primary vertex resolutions (μm)			B^0 vertex resolutions (μm)		
	x	y	z	x	y	z
1.00000	9	9	41	14	14	147
1.00003	9	9	42	14	14	147
1.00010	9	9	42	14	14	145
1.00033	9	9	46	14	14	149
1.00100	11	11	72	16	15	184

Table 21: Values of the resolutions of the primary and the B^0 decay vertices for the various VELO z-scaling scenarios. The errors on all resolutions are around 1-1.5 %.

Looking at the pull distributions for the reconstructed proper time shown in Figure 18 and their summary in Table 22, it appears that there is no significant change in the proper time bias due to a change in the z scale. This is expected as, even for the largest z-scale under study, the estimated effect on the pull mean is of the order of its uncertainty.

z-scale	Mean	Sigma
1.00000	0.06 ± 0.02	1.14 ± 0.01
1.00003	0.06 ± 0.02	1.15 ± 0.01
1.00010	0.07 ± 0.02	1.15 ± 0.02
1.00033	0.07 ± 0.02	1.15 ± 0.01
1.00100	0.05 ± 0.02	1.35 ± 0.02

Table 22: Values for the mean and sigma of the proper time pulls for the various VELO z-scaling scenarios.

4 Conclusions

In this note an extensive study of the effects of misalignments of the tracking stations on the analysis of B decays has been presented, illustrated by the example channel of $B^0_{(s)} \to h^+h'^-$.

The effects of the VELO and of the downstream tracking stations IT and OT are rather decoupled. A summary for various quantities related to the B^0 candidates is given in Table 23.

	Affected by VELO misalignments	Affected by T misalignments
B^0 daughters momentum	no	yes
B^0 mass	no	yes
B^0 vertex	yes	no
B^0 impact parameter	yes	no
B^0 proper time	yes	no

Table 23: Summary of the combined effect of misalignments in the VELO and the T-stations on various physics quantities involved in the selection of $B^0_{(s)} \to h^+h'^-$ events.

This study has shown that misalignments of the order of one third of the detector single-hit resolutions (our "1σ" scales) have little or negligible effects on the quality of the reconstruction and of the analysis of $B^0_{(s)} \to h^+h'^-$ decays.

The impact of misalignments on the performance of the pattern recognition algorithms and on the primary vertex resolutions has also been assessed for the first time. It is important to realise that these quantitative results obtained are rather general and not restricted to $B^0_{(s)} \to h^+h'^-$ decays – they are independent of the actual B decay.

A natural follow-up study would involve the assessment of residual effects after application of the several dedicated alignment algorithms being developed at present. Preliminary studies with the latest versions of the algorithms seem to indicate a performance leading to residual misalignments of the order of our "1σ" scales. A detailed discussion is left for a future analysis.

A Comments on misalignments sub-samples

As explained in Section 2, all $20k$ samples of each scenario considered have been produced as 10 sub-samples of $2k$ events, each of which using a different set of the 10 sets of a particular misalignment scenario. This procedure was chosen to avoid any potentially "friendly" or "catastrophic" set of misalignments.

Figures 19, 20, 21 and 22 exemplify the distributions (over the 10 sets) of pattern recognition efficiencies for the `Matching`and the `Forward`algorithms respectively for the 0σ case and for the 5σ misalignments cases of the VELO, the T-stations, and the VELO and T-stations. Pattern recognition efficiency variations of the order of a few percent are observed on a per sub-sample basis.

Furthermore, regarding the measurement of resolutions it can be argued that when averaging over 10 samples of different misalignments one measures not only the average resolution but also a contribution coming from the spread of a potential bias in the single samples. To assess the size of this effect the resolutions and biases have been measured on each of the 10 samples. Thereafter, the average resolution was compared to the spread of the observed biases by taking a ratio of these quantities. In the ideal case of a negligible bias this ratio would take values larger than 1. Over all the resolutions under study this quantity varied between 14 and 36 in the 0σ case and between 3 and 15 in the 5σ case. This means that even in the worst case the contribution of the variation in the bias is a factor 3 smaller than the average resolution. When combining these numbers, by naively adding them in quadrature, one arrives at the conclusion that a variation in the bias of the single misalignment samples should account for at most 10% of the measured resolution. Hence the method of averaging over 10 samples of different misalignments is valid and does not lead to significantly wrong results.

References

[1] The LHCb Collaboration, S.Amato $et\ al.$,*LHCb Techical Proposal*, CERN/LHCC 1998-04, 1998.

[2] The LHCb Collaboration, Nobrega R. $et\ al.$, *LHCb Reoptimized Detector Design and Performance Technical Design Report*, CERN-LHCC/2003-030, 2003.

[3] D. Petrie $et\ al.$, *Study of the impact of VELO misalignments on the LHCb tracking and L1 trigger performance*, LHCb Note 2005-056, 2005.

[4] J. Nardulli, *Reconstruction of two-body B decays in LHCb*, CERN-THESIS 2007-063.

[5] A. Carbone $et\ al.$, *Charmless charged two-body B decays at LHCb*, LHCb Note 2007-056, 2007;
A. Carbone $et\ al.$, *Analysis of two-body B decays at LHCb using DC06 data*, LHCb Note in preparation.

[6] M. Needham, *Performance of the LHCb track reconstruction software*, LHCb Note 2007-144, 2007.

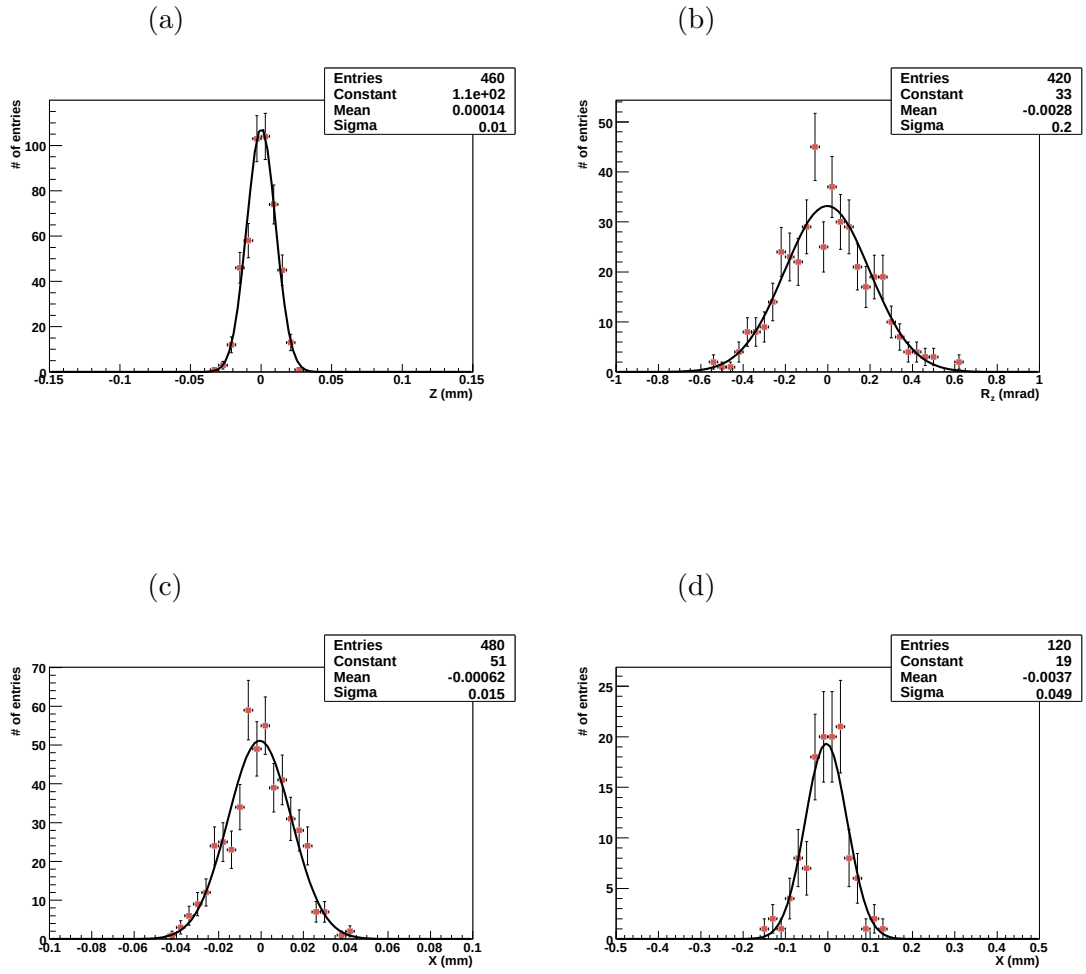

Figure 2: Gaussian distributions for the 1σ misalignment scales introduced in the conditions databases for (a) VELO modules z translations, (b) VELO sensors z rotations, (c) IT boxes x translations and (d) OT layers x translations.

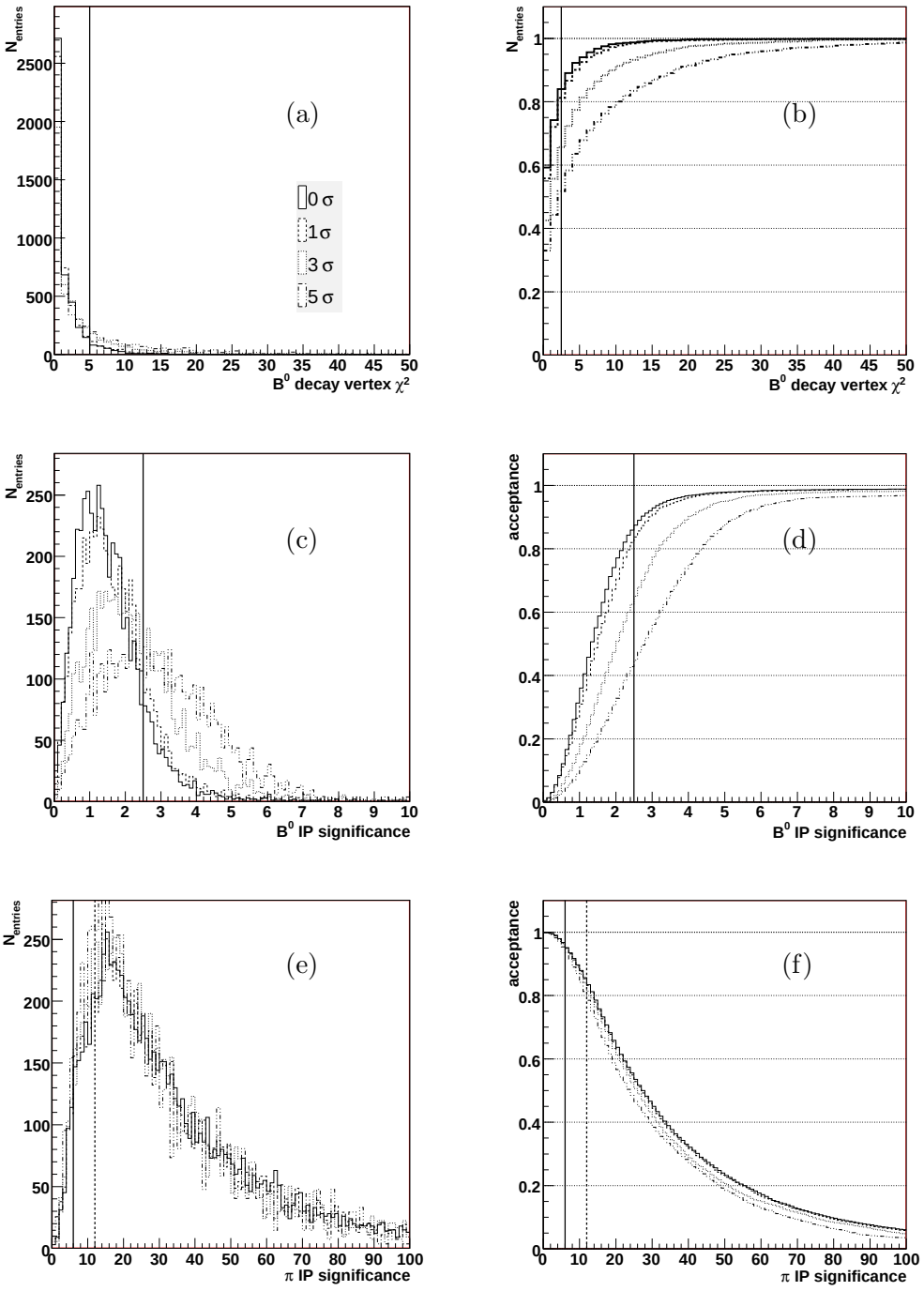

Figure 3: Effect of VELO misalignments on the B^0 decay vertex χ^2 and impact parameter significances for the B^0 candidate and its daughter pions. The right-hand-side distributions correspond to the integrated left-hand-side distributions. The full line represents the 0σ misalignment scenario; the dashed line represents the 1σ scenario; the dotted line represents the 3σ scenario and the dot-dashed line represents the 5σ scenario. The vertical cut lines are detailed in Section 3.1.2.

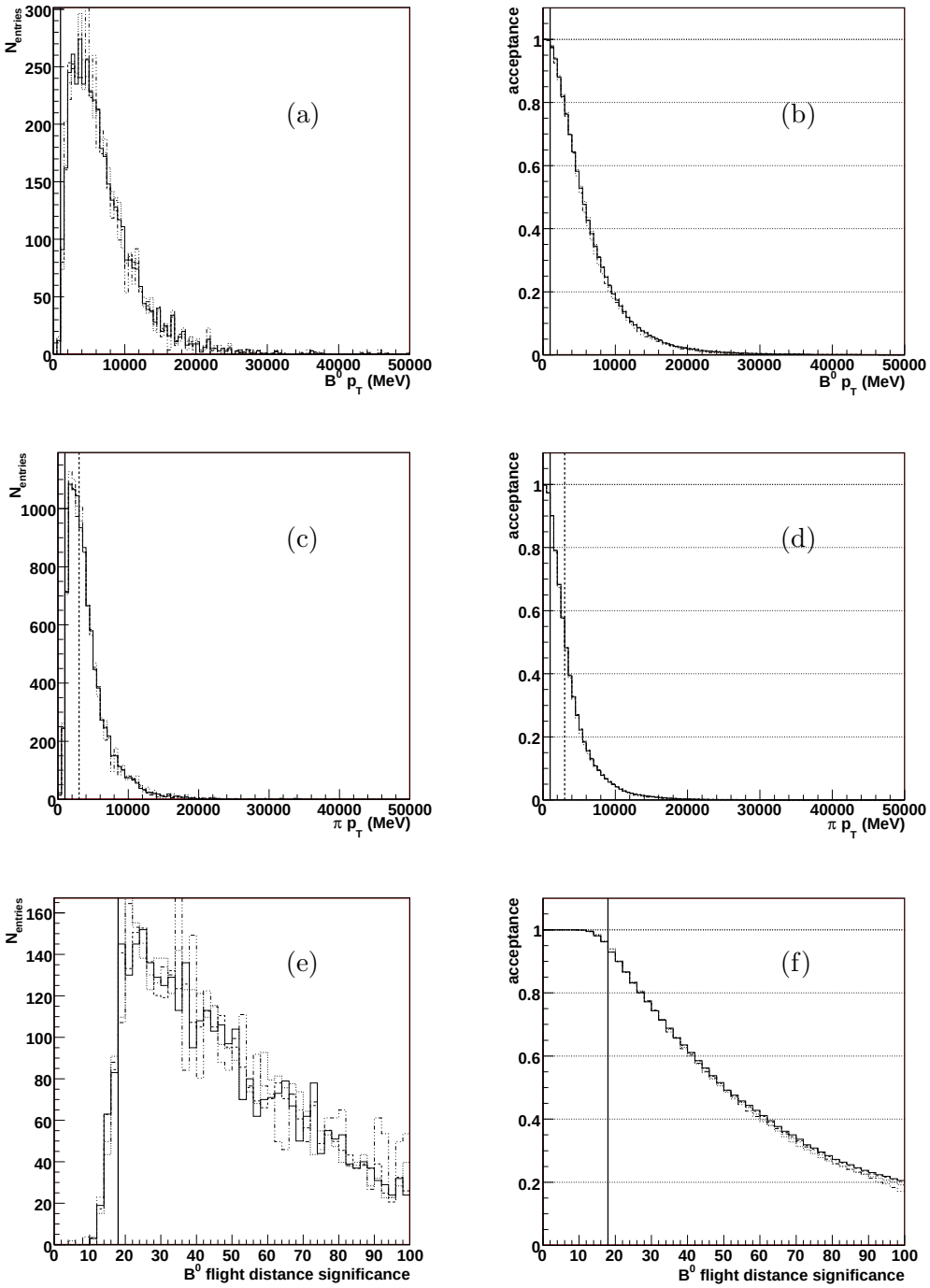

Figure 4: Effect of VELO misalignments on the transverse momentum of the B^0 and daughter pions, and B^0 flight distance significance. The right-hand-side distributions correspond to the integrated left-hand-side distributions. The various line styles are as explained in Figure 3. The vertical cut lines are detailed in Section 3.1.2.

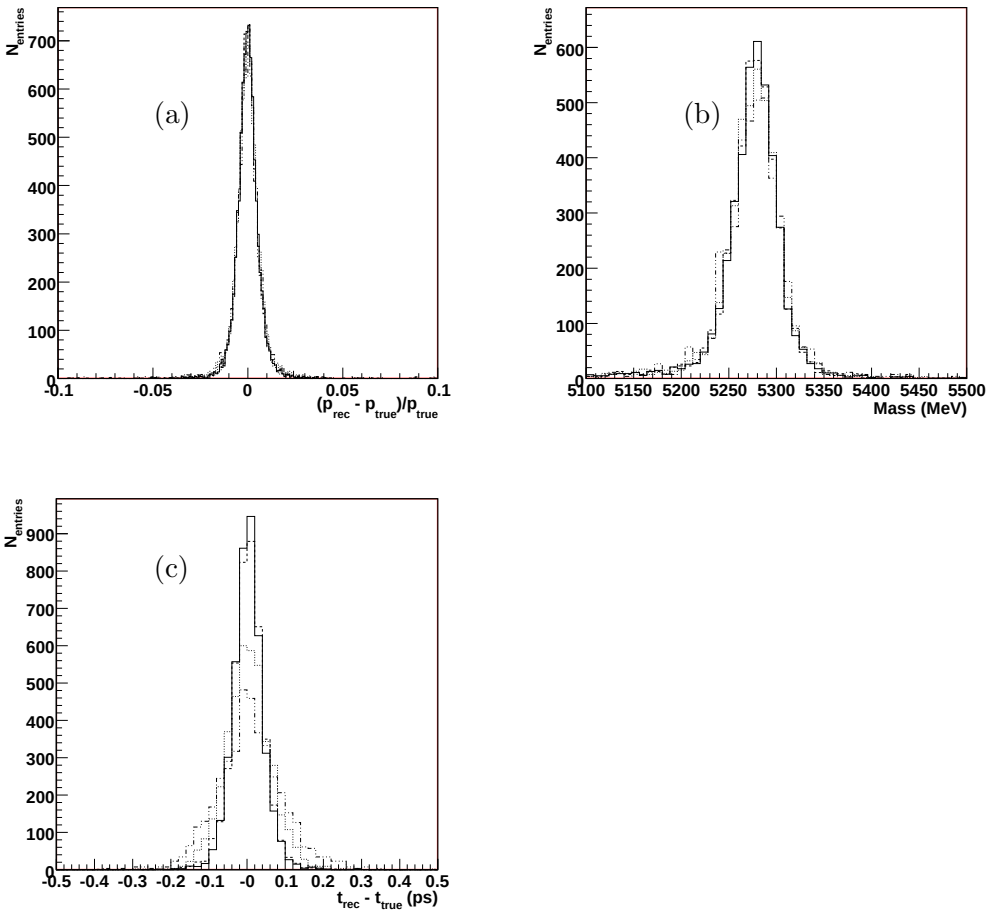

Figure 5: Effect of VELO misalignments on the resolutions in (a) momentum of the daughter pions, in (b) B^0 invariant mass and in (c) B^0 proper time. The various line styles are as explained in Figure 3.

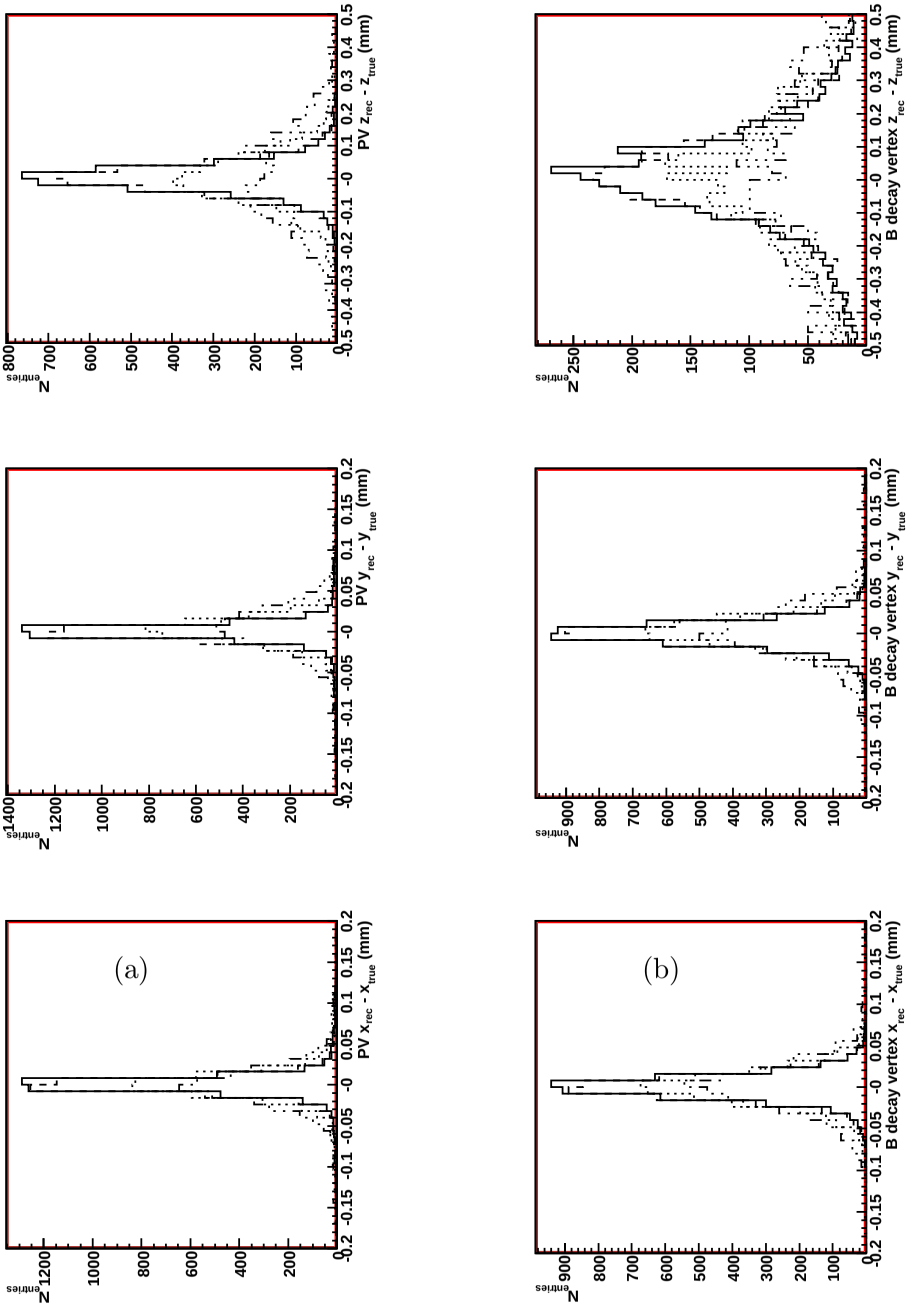

Figure 6: Effect of VELO misalignments on the resolutions of the (a) primary vertex and (b) the B^0 vertex. The various line styles are as explained in Figure 3.

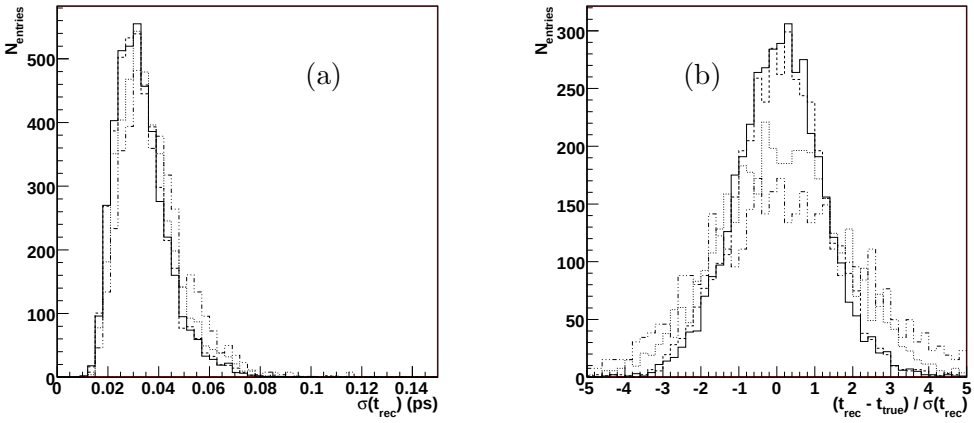

Figure 7: Effect of VELO misalignments on (a) the B^0 proper time error and (b) on the pull distribution of the B^0 proper time. The various line styles are as explained in Figure 3.

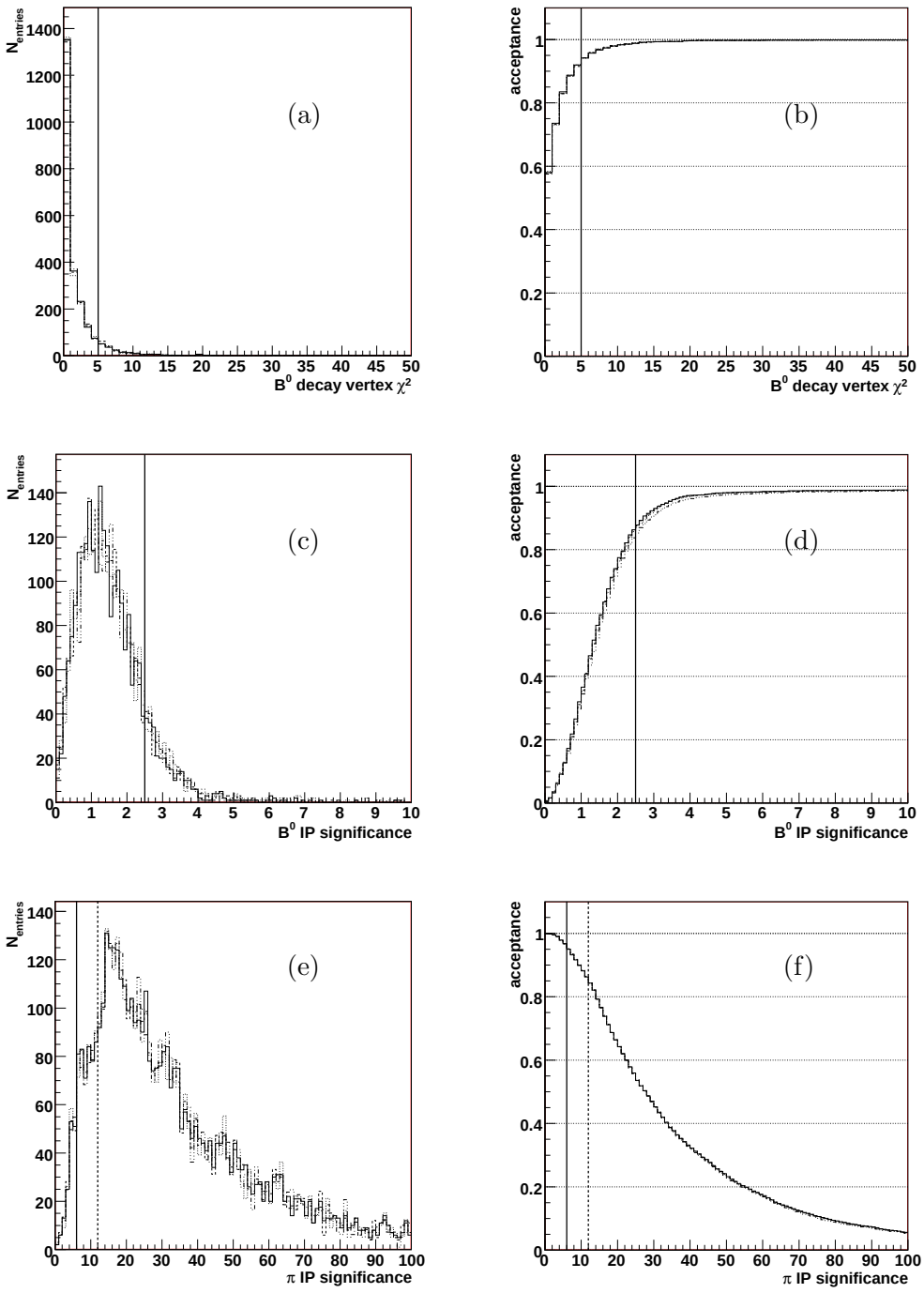

Figure 8: Effect of T-stations misalignments on the B^0 decay vertex χ^2 and impact parameter significances for the B^0 candidate and its daughter pions. The right-hand-side distributions correspond to the integrated left-hand-side distributions. The various line styles are as explained in Figure 3. The vertical cut lines are detailed in Section 3.1.2.

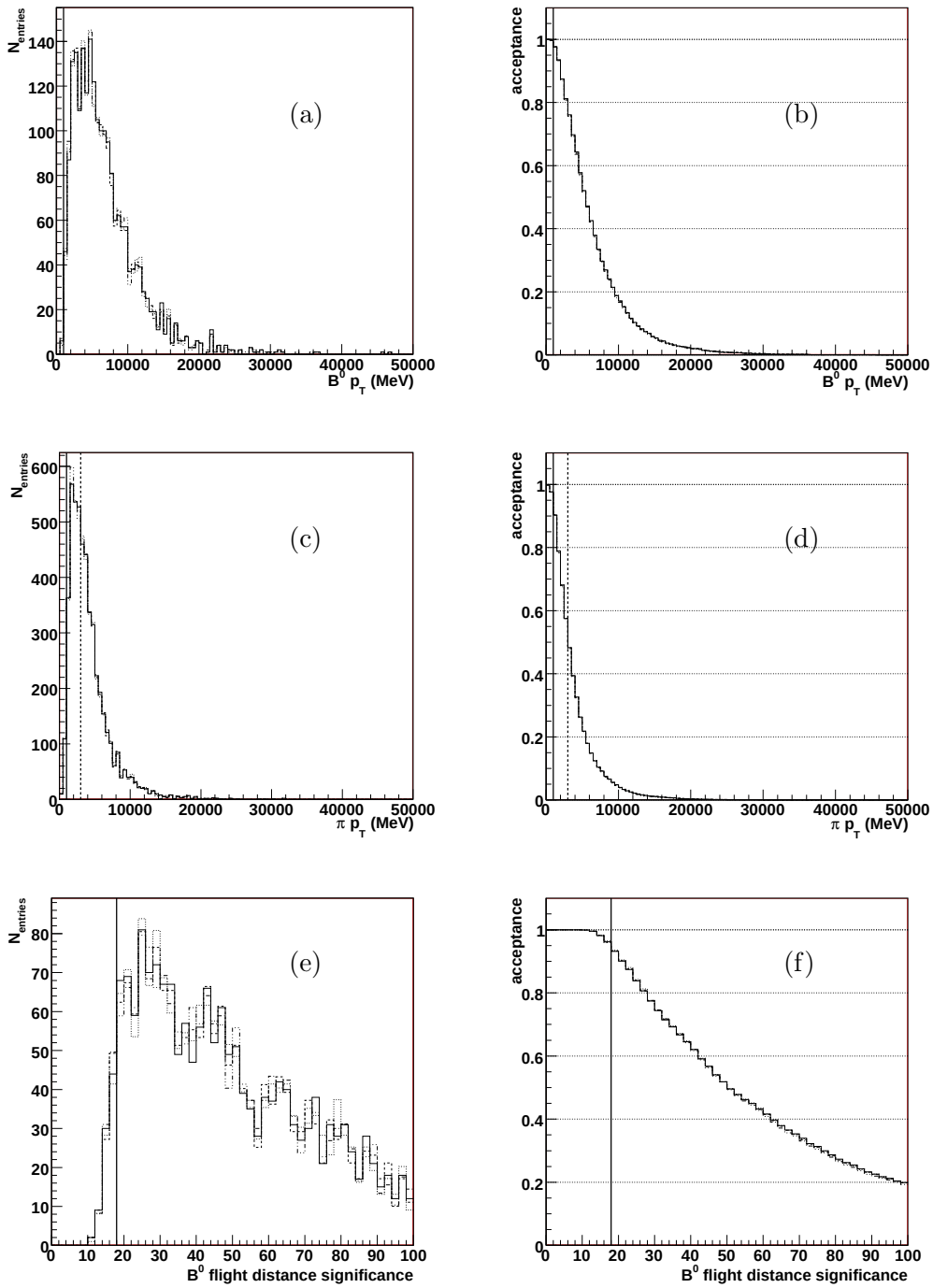

Figure 9: Effect of T-stations misalignments on the transverse momentum of the B^0 and daughter pions, and B^0 flight distance significance. The right-hand-side distributions correspond to the integrated left-hand-side distributions. The various line styles are as explained in Figure 3. The vertical cut lines are detailed in Section 3.1.2.

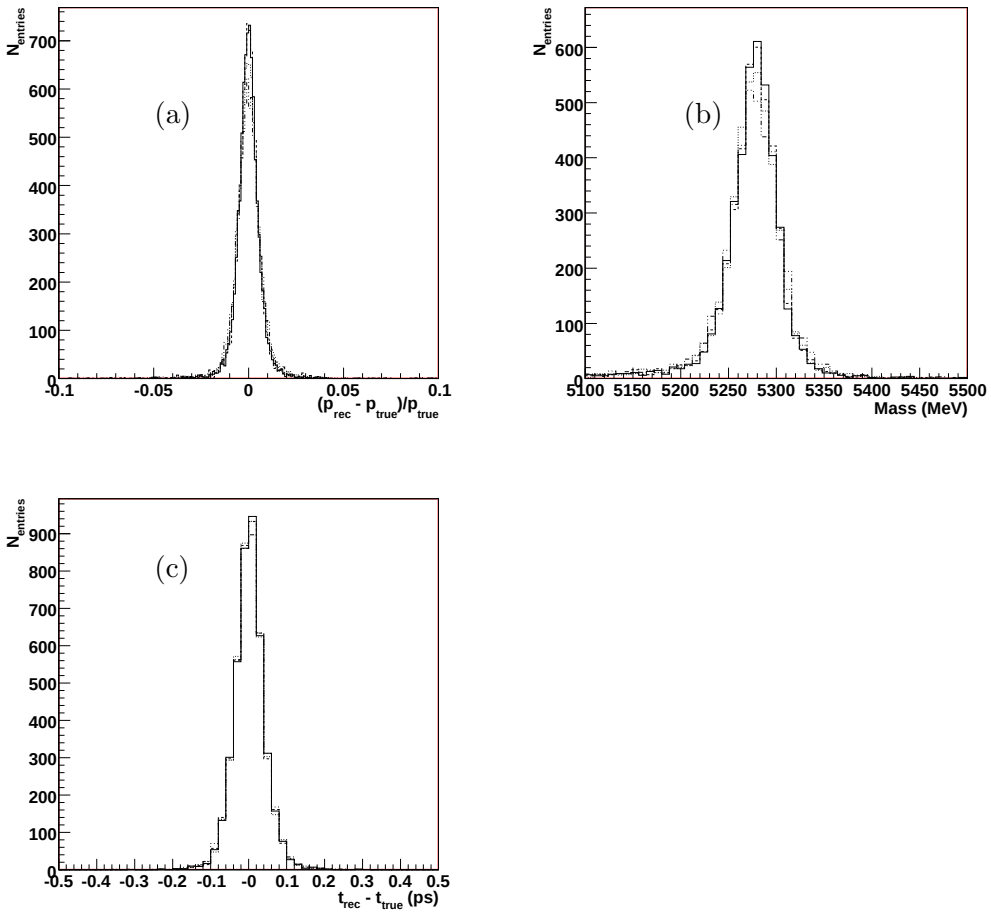

Figure 10: Effect of T-stations misalignments on the resolutions in (a) momentum of the daughter pions, in (b) B^0 invariant mass and in (c) B^0 proper time. The various line styles are as explained in Figure 3.

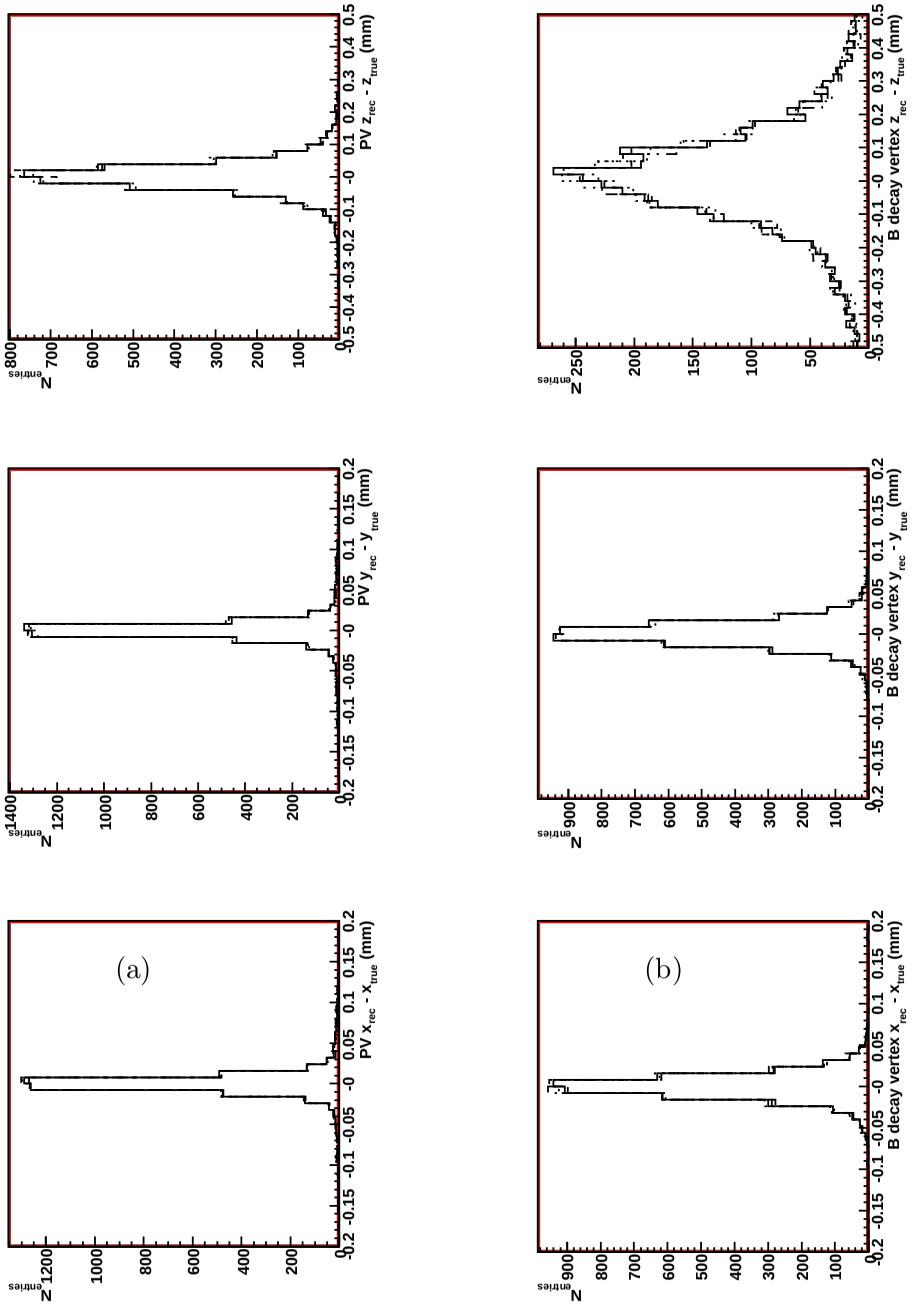

Figure 11: Effect of T-stations misalignments on the resolutions of the (a) primary vertex and (b) the B^0 vertex. The various line styles are as explained in Figure 3.

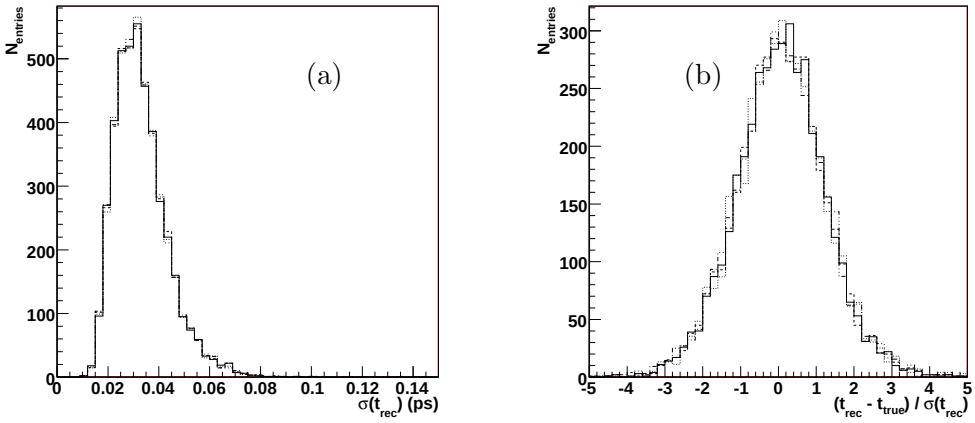

Figure 12: Effect of T-stations misalignments on (a) the B^0 proper time error and (b) on the pull distribution of the B^0 proper time. The various line styles are as explained in Figure 3.

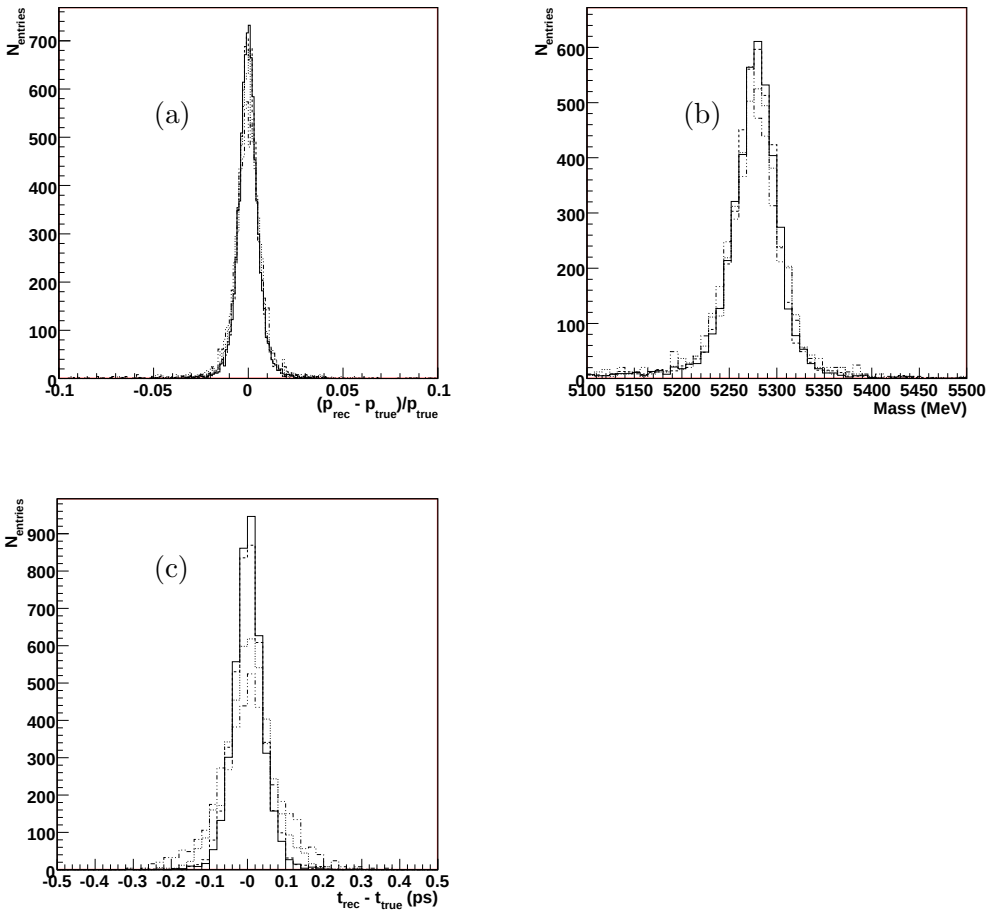

Figure 13: Effect of VELO and T-stations misalignments on the resolutions in (a) momentum of the daughter pions, in (b) B^0 invariant mass and in (c) B^0 proper time. The various line styles are as explained in Figure 3.

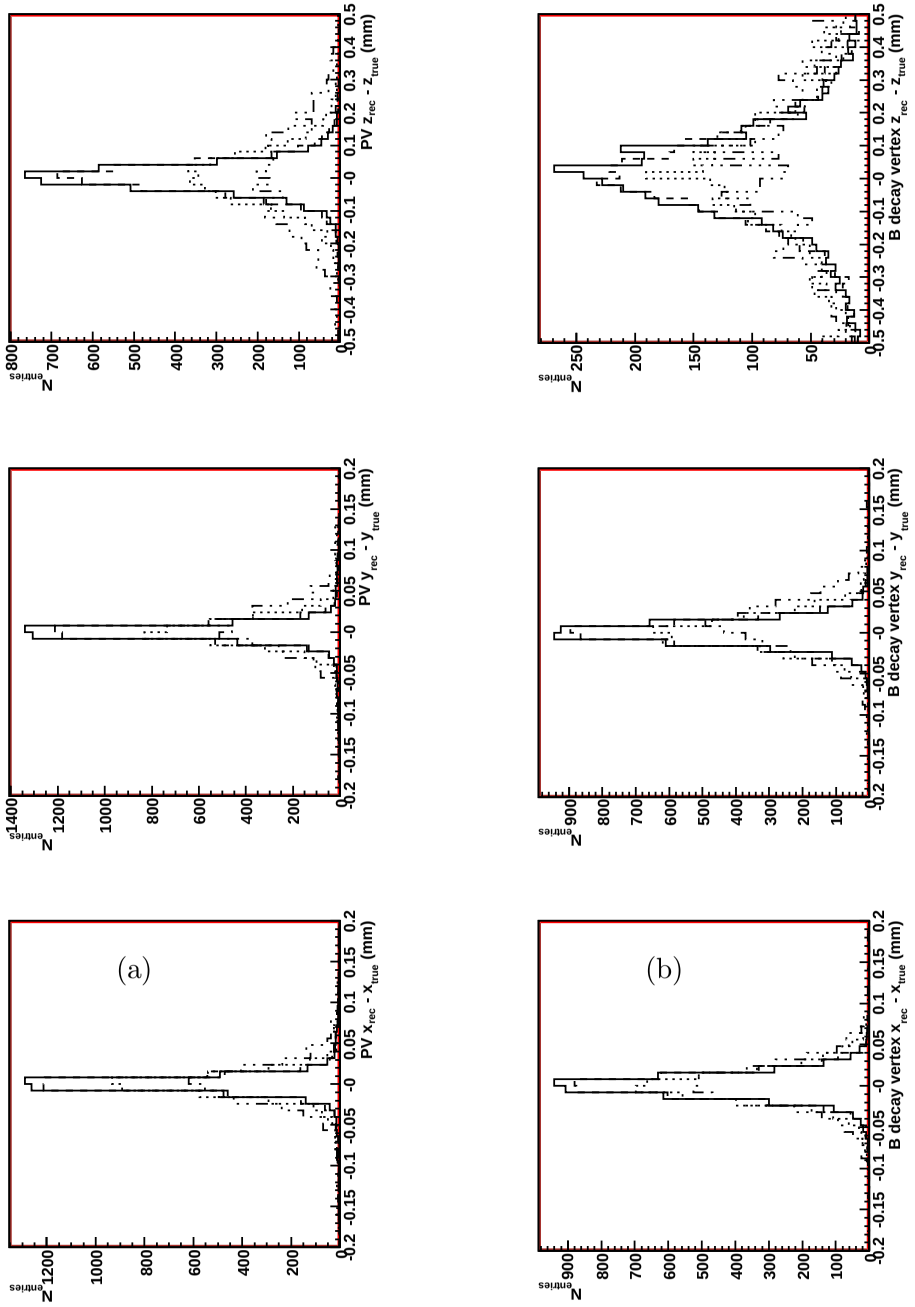

Figure 14: Effect of VELO and T-stations misalignments on the resolutions of the (a) primary vertex and (b) the B^0 vertex. The various line styles are as explained in Figure 3.

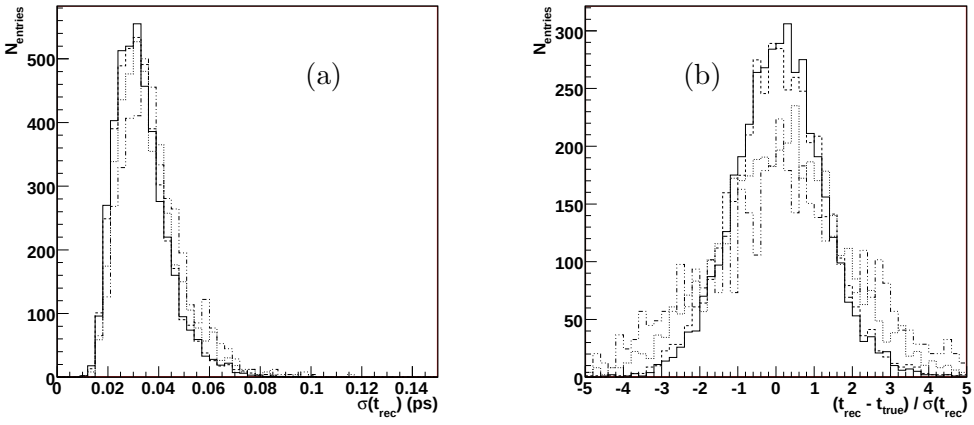

Figure 15: Effect of VELO and T-stations misalignments on (a) the B^0 proper time error and (b) on the pull distribution of the B^0 proper time. The various line styles are as explained in Figure 3.

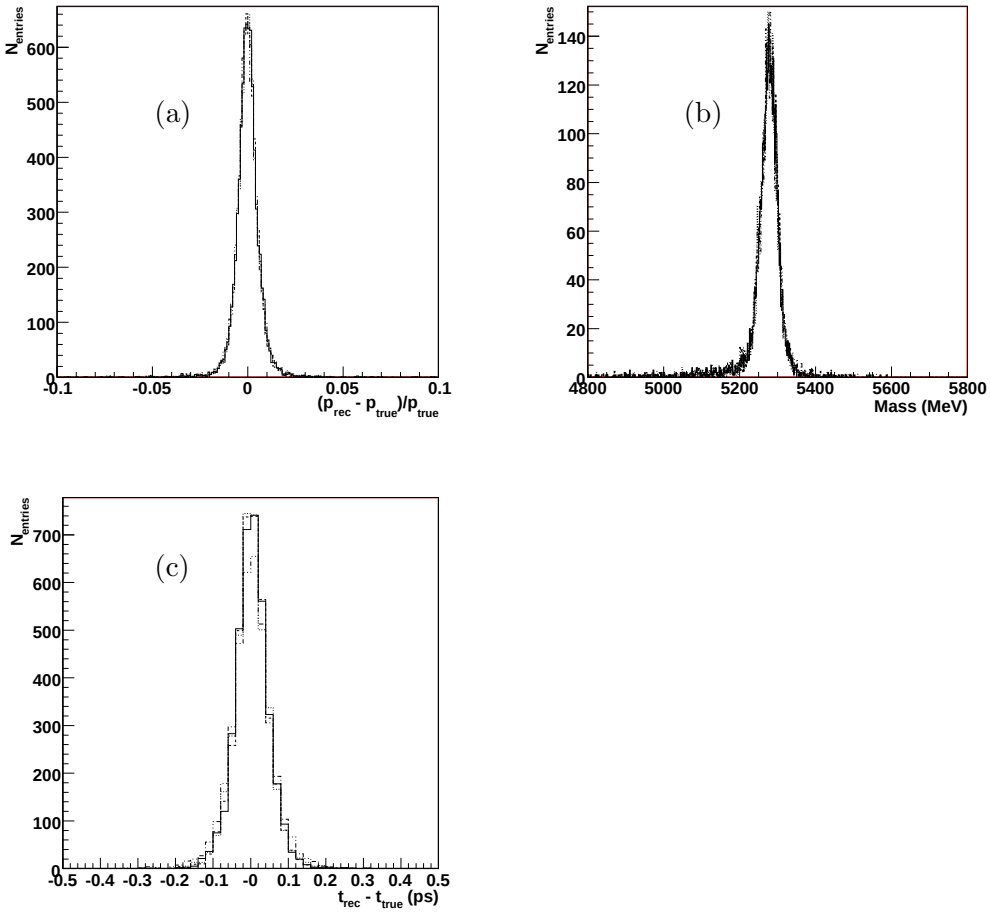

Figure 16: Effect of VELO z-scaling misalignments on the resolutions in (a) momentum of the daughter pions, (b) B^0 invariant mass and in (c) B^0 proper time. The full line corresponds to a z-scale of 1.00003; the dashed line corresponds to a z-scale of 1.00010; the dotted line corresponds to a z-scale of 1.00033 and the dot-dashed line corresponds to a z-scale of 1.00100.

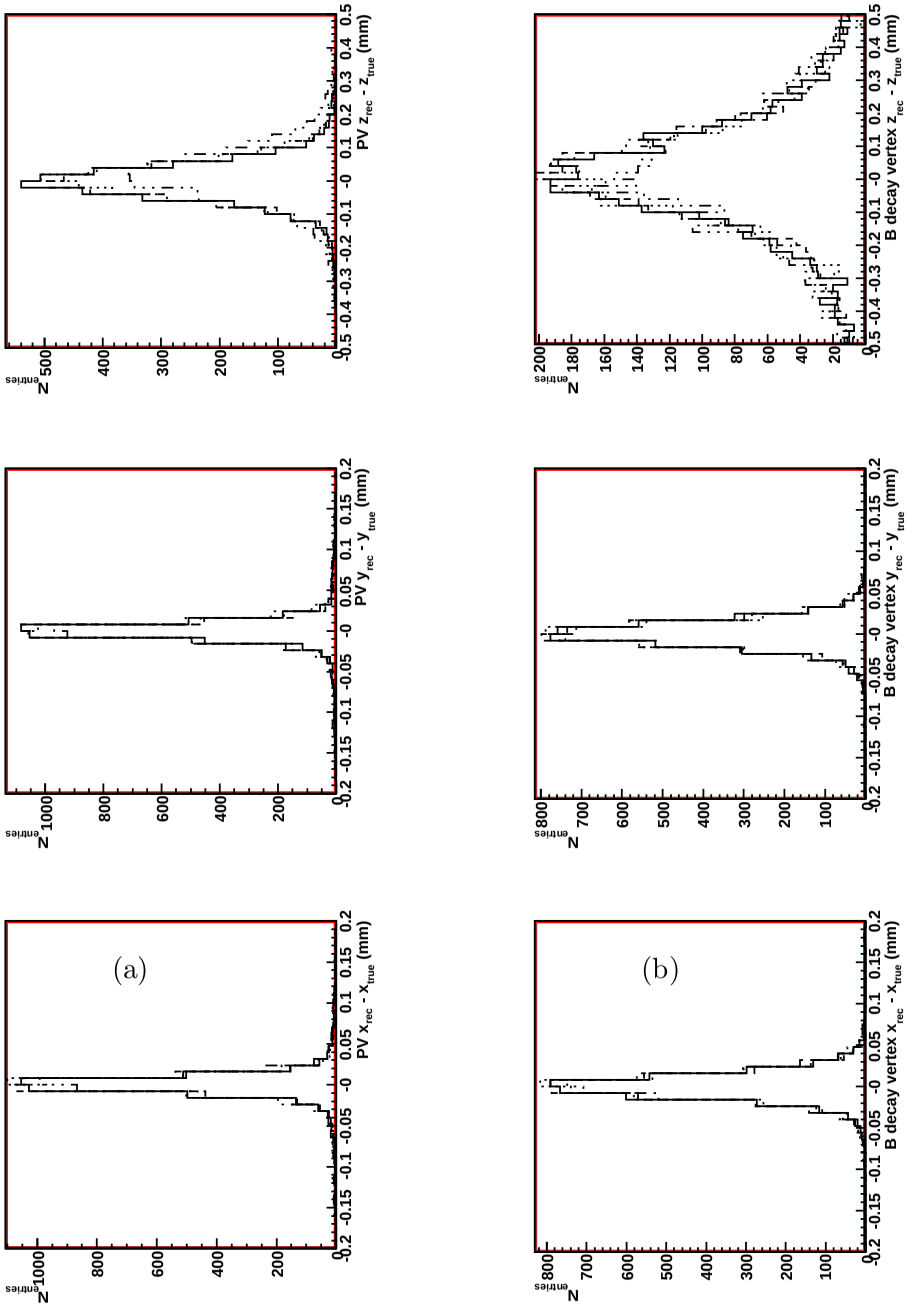

Figure 17: Effect of VELO z-scaling misalignments on the resolutions of the (a) primary vertex and (b) the B^0 vertex. The various line styles are as explained in Figure 16.

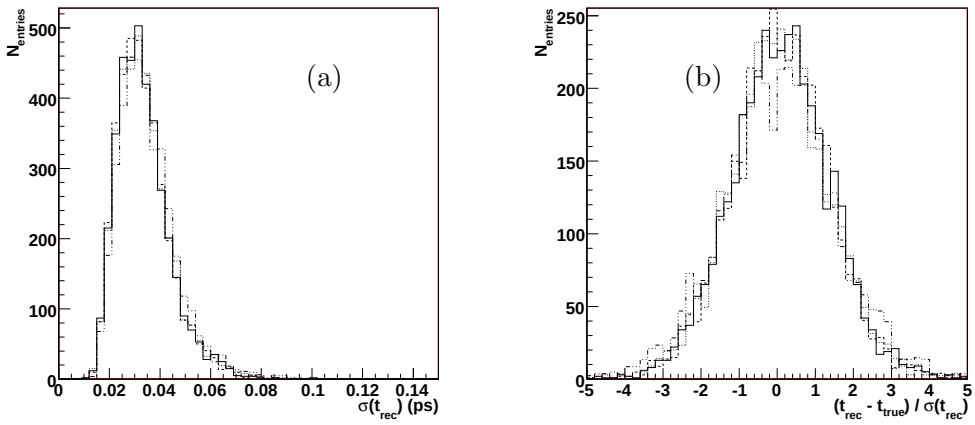

Figure 18: Effect of VELO z-scaling misalignments on (a) the B^0 proper time error and (b) on the pull distribution of the B^0 proper time. The various line styles are as explained in Figure 16.

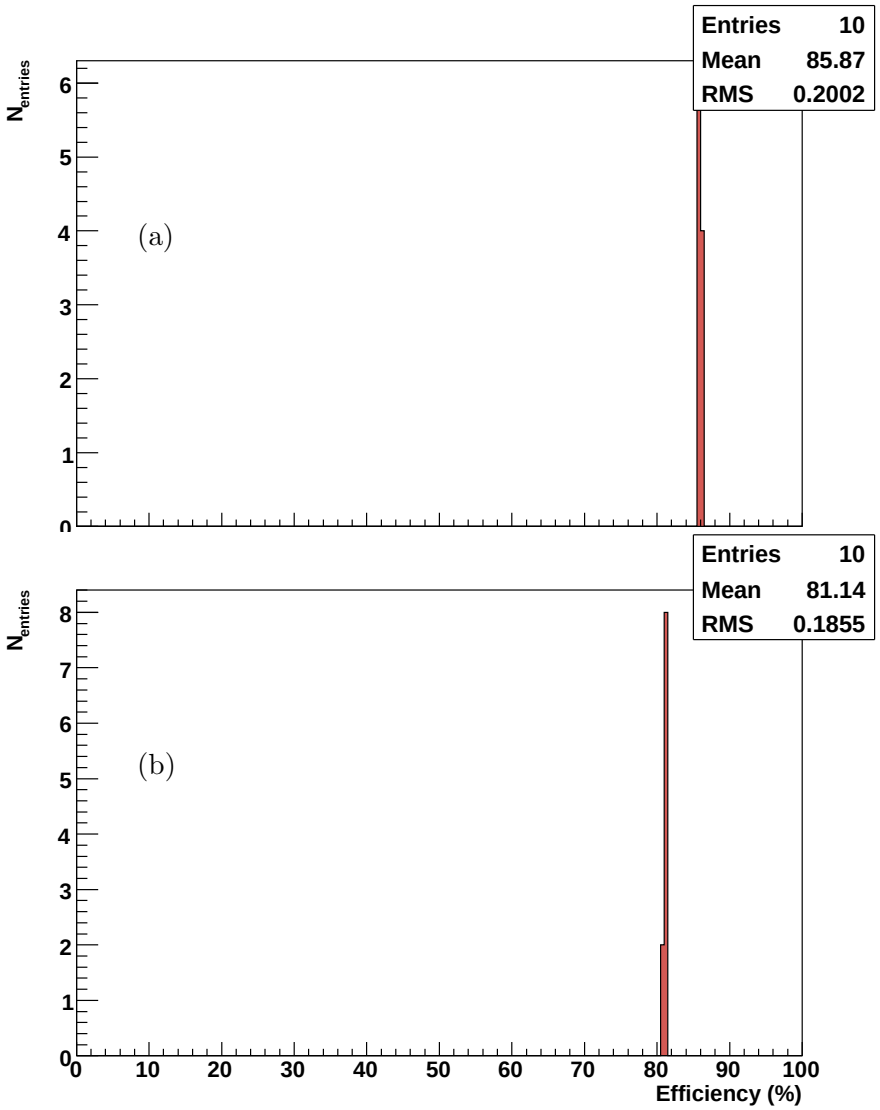

Figure 19: Pattern recognition efficiencies with a perfect alignment for (a) the `Forward` and (b) the `Matching` algorithms.

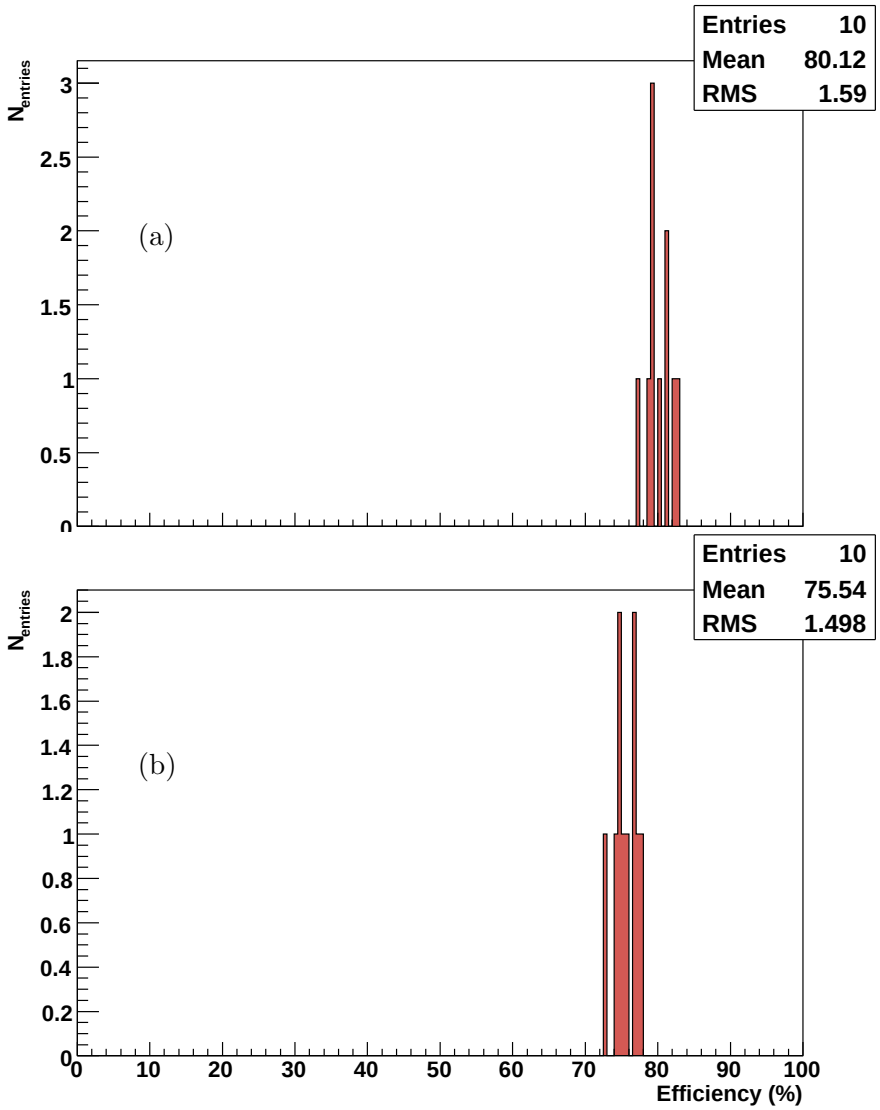

Figure 20: Pattern recognition efficiencies with 5σ misalignments of the VELO for (a) the `Forward` and (b) the `Matching` algorithms.

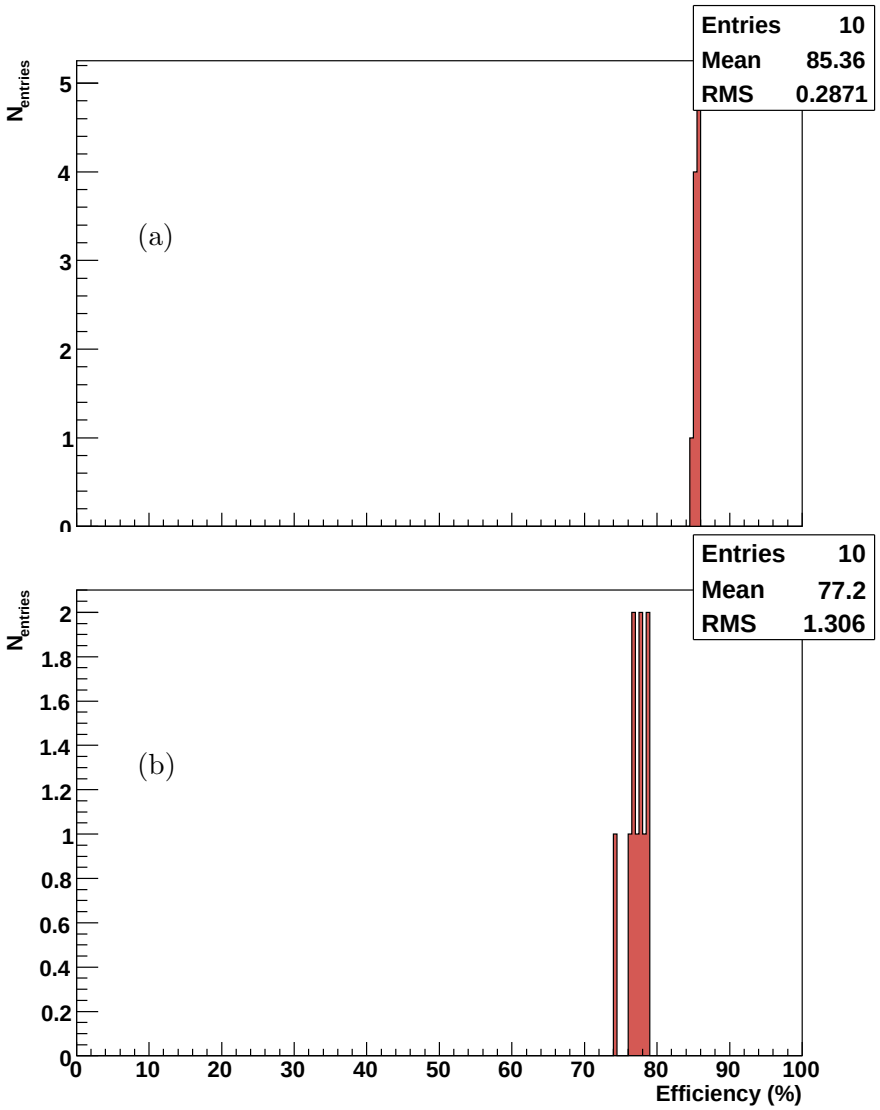

Figure 21: Pattern recognition efficiencies with 5σ misalignments of the T-stations for (a) the `Forward` and (b) the `Matching` algorithms.

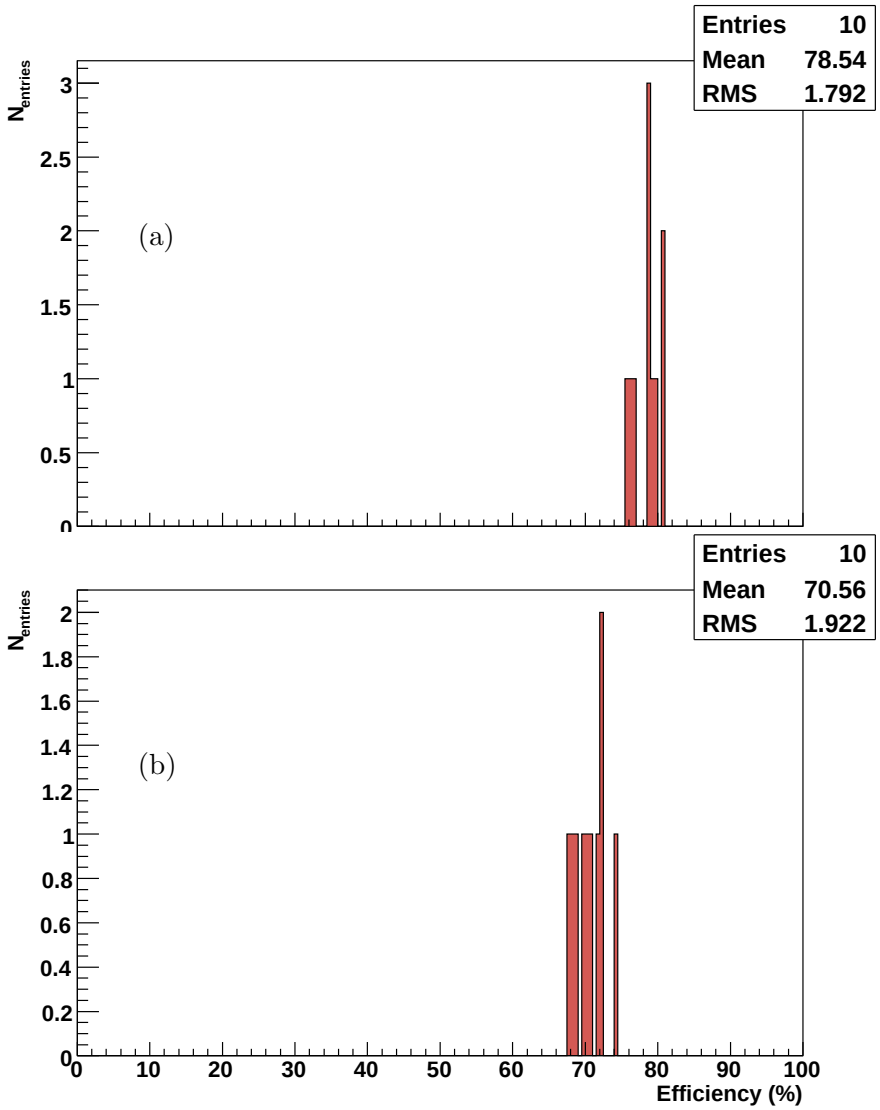

Figure 22: Pattern recognition efficiencies with 5σ misalignments of the VELO and the T-stations for (a) the `Forward` and (b) the `Matching` algorithms.